Wei Xin (Orcid ID: 0000-0003-3616-3031)
Chan Pak Wah (Orcid ID: 0000-0003-1843-5566)
Kuang Zhiming (Orcid ID: 0000-0001-9017-0350)

# Two-Point Mixing, Buoyancy Sorting and Updraft Dilution in the RACORO Campaign

**Xin Wei[1], Pak Wah Chan[1*], and Zhiming Kuang[1,2]**

[1]Department of Earth and Planetary Sciences, Harvard University, Cambridge, MA, USA.

[2]John A. Paulson School of Engineering and Applied Sciences, Harvard University, Cambridge, MA, USA.

[*]Current affiliation: College of Engineering, Mathematics and Physical Sciences, University of Exeter, Exeter, UK.

Corresponding author: Xin Wei (davidwei@g.harvard.edu)

**Key Points:**

- Aircraft measurements of shallow cumuli show two-point mixing but no ongoing buoyancy sorting.
- Around half of the instances of two-point mixing show no noticeable updraft dilution.
- Including surface heterogeneity yields better agreement of the cloud-layer horizontal moisture variation between LES and observations.

This article has been accepted for publication and undergone full peer review but has not been through the copyediting, typesetting, pagination and proofreading process which may lead to differences between this version and the Version of Record. Please cite this article as doi: 10.1029/2020GL090674

**Abstract**

Aircraft measurements of shallow cumulus cases from the RACORO campaign are studied in a transformed Paluch diagram. Previous studies have interpreted samples in Paluch diagrams in terms of two-point mixing and buoyancy sorting. The two-point mixing behavior is frequently seen in the RACORO observations and can be unambiguously distinguished from buoyancy sorting. The latter is not found in the RACORO observations and is also rare in a large-eddy simulation (LES) of a RACORO case. As opposed to often assumed gradual dilution of updrafts, around half of the instances of two-point mixing show no clear evidence of updraft dilution. We also find substantial spread in the properties of parcels that have adjusted to their level of neutral buoyancy and that a LES with horizontally homogeneous surface underestimates this spread. The inclusion of surface heterogeneity in the LES improves the agreement of its horizonal moisture variations with the aircraft measurements.

**Plain Language Summary**

Previous studies have proposed two-point mixing and buoyancy sorting to describe cloud dynamics. Using a mixing diagram to analyze aircraft measurements of temperature and moisture in shallow clouds and their surroundings, and taking non-cloudy air into account, we identify the two-point mixing scenario but find no instance of buoyancy sorting. Fingerprints of mixing between clouds and environment, as well as vertical air displacement driven by buoyancy, are identified. Cloudy updrafts experience no noticeable dilution in around half of the two-point mixing instances. Surface heat flux variations enhance the cloud-layer horizontal variation of moisture and increase overall cloud fraction.

## 1 Introduction

Cumulus convection and associated clouds are a major source of uncertainty in many aspects of the current climate models. They are identified as a major source of the uncertainty in projections of climate change (e.g., Bony & Dufresne, 2005). Deficiencies in cumulus parameterizations also contribute to biases such as the onset of precipitation over land being too early (e.g., Dai, 2006; Guichard et al., 2004), inability to simulate the Madden-Julian Oscillation (e.g., Del Genio, 2012; Lin et al., 2006), and the double-ITCZ bias (e.g., Lin, 2007; Mechoso et al., 1995), among others. Moreover, cumulus clouds are turbulent flows with phase transitions and have fascinating dynamics in their own right. A better understanding of their dynamics is of intrinsic intellectual value.

Historically, a number of studies have analyzed *in situ* aircraft measurements using 2-D diagrams of conserved variables, known as Paluch diagrams following Paluch (1979), to study the dynamics of cumulus clouds. Böing et al. (2014) provides a good discussion of past uses of such diagrams. Briefly, early Paluch diagrams of aircraft measurements were used as evidence for cloud top entrainment because the measured points tend to form a line between properties at the cloud base and the cloud top (Boatman & Auer Jr, 1983; Jensen et al., 1985; LaMontagne & Telford, 1983; Paluch, 1979; Reuter & Yau, 1987). Later studies, however, identified data biases that affect the conclusions reached in earlier work (Grabowski & Pawlowska, 1993; Malinowski & Pawlowska, 1989), while other studies such as Blyth et al. (1988) found mixing lines that connect the cloud base and a level close to the observational level, providing evidence for lateral mixing and the conceptual model of a shedding thermal. Furthermore, Taylor and Baker (1991) questioned the two-point mixing interpretation of straight-line behaviors in the Paluch diagram. They noted that the two conserved variables used in the Paluch diagrams are total water and the equivalent or liquid water potential temperature, which are often well correlated in the sounding. They argued that the measurements could not distinguish two-point mixing from buoyancy sorting that occurs as

mixed parcels adjust to their level of neutral buoyancy (Taylor & Baker, 1991). In sum, research on cumulus clouds faced a challenge with respect to the task of understanding the relationship between two-point mixing and buoyancy sorting.

Heus et al. (2008) devised a transformed Paluch diagram that allows two-point mixing to be more clearly distinguished from buoyancy sorting. They chose total water and a linear combination of the equivalent potential temperature and the liquid water potential temperature as the two conserved variables and adjusted the weights for the linear combination to minimize the correlation between the two. Heus et al. (2008) made transformed Paluch diagrams of the outputs of LES simulations of shallow cumuli and showed clear evidence of two-point mixing with source heights close to the observational levels, consistent with the conclusions from Blyth et al. (1988) and pointing to the importance of lateral mixing. No such analysis however has been applied to aircraft measurements.

The conventional Paluch diagram analyses have been conducted for samples *in clouds*, with aircraft sampling often aimed at the rising turrets of growing clouds. This was also partially due to the difficulties in measuring humidity of unsaturated air back then (e.g., Taylor & Baker, 1991). Such measurements played a key role in providing us with conceptual models of the mixing processes such as the shedding thermal model (Blyth et al., 1988). Going beyond such conceptual models, we are also interested in how high updrafts can reach without significant mixing with their environment. Such mixing between updrafts and their environment will be referred to as updraft dilution. We consider updraft dilution is detectable at a specific altitude if an updraft which has undergone mixing with the environment at substantially lower altitudes continues to rise to this altitude. The prevalence of updraft dilution is best quantified by statistically *unbiased* sampling, for example, with predetermined flight patterns. Moreover, since the cloud fraction in shallow cumulus convection is typically only a few percent (e.g., Siebesma et al., 2003), most of the air in a typical convective layer within which the cumuli are embedded is not cloudy and non-cloudy air can be the remnants of dissipated clouds (after all condensates have evaporated) or the unsaturated portion of the mixture between the updraft and the environment. Therefore, there potentially is value in including non-cloudy parcels in the analysis.

The goal of the present study is twofold. First, we shall revisit the issue of buoyancy sorting versus two-point mixing by applying the transformed Paluch diagram analysis to the aircraft data from the RACORO campaign, which features predetermined flight patterns and modern instrumentation. Second, we will explore the value of including non-cloudy parcels in the Paluch diagram analysis. As we shall see, the inclusion of non-cloudy parcels makes it easier to identify the two-point mixing behavior and to determine if an updraft is diluted without necessarily capturing the updraft during the flight; it also shows the adjustment to the level of neutral buoyancy (i.e. the buoyancy sorting process). The observational analysis is further augmented by large-eddy simulations (LES) with Lagrangian particle tracking, which will be used to aid the interpretation of and provide broader context to the RACORO observations. We will limit ourselves to shallow convection in this initial study for its relative simplicity compared to deep convection.

The remainder of the paper is structured as follows. Section 2 briefly introduces the RACORO campaign, the setups of three LES and the transformed Paluch diagram. Section 3 discusses four scenarios in the observations and LES, namely, two-point mixing, neutral buoyancy, buoyancy sorting and downdraft overshooting. Section 4 addresses the question of updraft dilution with the aircraft and surface measurements. Section 5 studies model biases related to surface heterogeneity. The conclusion and discussion are presented in section 6.

## 2 Data and Methods

### 2.1 Observations

RACORO (Routine Atmospheric Radiation Measurement (ARM) Aerial Facility (AAF) Clouds with Low Optical Water Depths (CLOWD) Optical Radiative Observations) was a comprehensive field campaign based on the ARM site on the southern great plain (SGP) from January 2009 to June 2009 (Vogelmann et al., 2012). During this campaign, in situ aircraft observations were made by the Twin Otter aircraft from the Center for Interdisciplinary Remote-piloted Aircraft Studies. A variety of boundary layer clouds, from stratus to shallow cumulus, were sampled by the aircraft. Temperature was measured by a Rosemount probe. Dew point temperature was measured by a Diode Laser Hygrometer. Liquid water content was obtained by a Gerber probe. When dew point temperature is erroneously higher than temperature, we cap the dew point temperature at temperature. Surface conditions were retrieved by a 25-m tower and Eddy Correlation Flux Measurement System at/around the ARM central facility (CF) at SGP. Vertical profiles were obtained by a balloon-borne sounding system, and an atmospheric emitted radiance interferometer (AERI), which are validated against the aircraft measurements during ascent/descent (Fig. S1).

We include samples that satisfy all four criteria: a) measuring cloud was (part of) the flight mission; b) samples were within 10 km from CF, where surface conditions and vertical profiles were measured; c) samples from the same flight at the same height were not completely homogeneous in the Paluch diagrams; and d) cloud fraction during the flight (from the data acquisition system images) had been less than 100% (otherwise the cloud layer is occupied by stratiform clouds and likely has little heterogeneity). 16 flights contain such qualified samples. For brevity, 6 of them are presented in Fig.1, and the rest are in Fig. S2.

### 2.2 Large-eddy simulations

This LES case was configured and studied by Endo et al. (2015) and Vogelmann et al. (2015). We use System for Atmospheric Modeling (SAM, Khairoutdinov & Randall, 2003) with a single-moment bulk microphysics scheme and Smagorinsky scheme for subgrid-scale mixing for the simulation (see Khairoutdinov & Randall, 2003 and references therein for more details of these schemes). SAM uses wind velocities, liquid water/ice moist static energy (MSE), total nonprecipitating water and total precipitating water as its prognostic variables. The longwave and shortwave calculation follows the Community Atmosphere Model (CAM, Collins et al., 2004) by National Center for Atmospheric Research (NCAR). The model calculates the solar zenith angle based on the latitude of the CF and local time. The doubly periodic domain measures 9.6 km in both x and y directions and 5.6 km in height. Although smaller than the standard ARM SGP observational domain, this domain is big enough to accommodate many shallow cumulus clouds (Zhang & Klein, 2013). Following Endo et al. (2015), the grid spacing is set to 75 m in the horizontal directions and 40 m in the vertical direction. The simulation is initialized at 6 am with the vertical profiles from the radiosonde launched at 5:30 am local time (LT = UTC - 6) on May 22, 2009. It is integrated for 6 hours with a time step of 2 s. The simulation is driven by large-scale forcing and surface heat fluxes from the ARM Continuous Variational Analysis (VARANAL) forcing product. Surface momentum flux is computed with Monin-Obukhov similarity with an aerodynamic roughness length of 0.04 m. Above the near-surface layers, the MSE and total nonprecipitating mixing ratio are nudged to their reference profiles from VARANAL on a 12-h timescale, and the horizontal wind velocities are nudged to their reference profiles on a 3-h timescale. More details of the simulation setup can be found in Endo et al. (2015). Shallow cumulus clouds are sampled at 11:30 am from the LES.

To demonstrate the effects of surface heterogeneity, we also devise an additional pair of LES with homogenous versus heterogeneous surface heat fluxes in an idealized manner. The domains of both LES are elongated in x direction (9 times the size in y). For the LES with heterogeneous surface fluxes, a square subdomain, 1/9 of the total area, is applied 50% higher surface sensible and latent heat fluxes than the rest of the domain. The domain average sensible/latent heat fluxes in the two LES are kept the same as in the original case. All other setups (spatial and temporal resolutions, radiation, relaxation and large-scale forcing) are identical to the original LES with a smaller domain. The LES with elongated domain and homogenous surface fluxes gives similar results as those from the original LES, suggesting that the altered domain size bears no impact on our results. The elongation of the domain, the patch size and the magnitude of surface flux perturbations are chosen to qualitatively reflect the length scale of the flight path and magnitude of surface flux variations. We compare the additional pair of LES in section 5 to study model biases related to surface heterogeneity.

### 2.3 Transformed Paluch diagram

Here we use a transformed Paluch diagram introduced by Heus et al. (2008) for the analyses. The transformed Paluch diagram is a scatterplot with total specific humidity ($q_t$) as its y axis and $T_\alpha$ as its x axis. $T_\alpha$ is defined as $0.272 \cdot \theta_e + 0.728 \cdot \theta_l$ where $\theta_e$ is the equivalent potential temperature and $\theta_l$ is the liquid potential temperature. The linear combination coefficients are empirically chosen as such to best separate the density isopleth from a two-point mixing line. For the LES results, moist static energy and liquid water static energy are used instead as they are the conserved variables in the model. But they are still labeled as $\theta_e$ and $\theta_l$ for the convenience of comparison. The density isopleths, the saturation lines, and the vertical sounding profiles, when appropriate, are also indicated on the diagram.

## 3 Mixing and Adjustment

### 3.1 Two-Point Mixing and Neutral Buoyancy

Consider the mixtures of two homogenous air masses. In a (transformed) Paluch diagram, such mixtures would fall on the line segment that connects the properties of the two air masses. This pattern is the so-called “two-point mixing”. The two air masses can be a cumulus updraft and the environment. The latter has neutral buoyancy and lies on the density isopleth. Subsequently, these mixtures displace vertically according to their buoyancy (buoyancy sorting) and mix with surrounding air by turbulence. Mixtures with strongly negative buoyancy become downdrafts, and are occasionally very penetrative, as we shall see later. Eventually these mixtures would achieve neutral buoyancy. If the turbulent mixing during and after the sorting is relatively weak, these mixtures would not collapse into a single point but distribute as a line on the density isopleth in a transformed Paluch diagram (hereafter the neutral buoyancy). Neutral buoyancy here can be viewed as the final stage of buoyancy sorting, while buoyancy sorting refers to the ongoing displacements of positively/negatively buoyant air.

Fig. 1 displays the samples from 6 flights in the transformed Paluch diagram. The rest of the flights of the RACORO campaign are included in Fig. S2. The two-point mixing and the neutral buoyancy are commonly seen in Fig. 1. Features of the neutral buoyancy can for example be found at levels 2 and 4 on May 13, where samples spread on the density isopleth. Two-point mixing, where samples distribute as a line not on the density isopleth, can be found on level 2 on March 30, level 1 on May 6, levels 2 and 3 on June 9, levels 4 and 5 on June 11, levels 1 and 4 on June 12 (Fig. 1), level 6 on May 23 (Fig. S2c), levels 1 and 5 on

May 24 (Fig. S2d), adding up to 11 instances. Later in section 4, we will discuss how these two-point mixing lines inform us about updraft dilution.

### 3.2 Example and Counterexamples of Buoyancy Sorting

Buoyancy sorting, according to Taylor and Baker (1991), assumes that a) the surrounding environment is homogenous, and b) parcels currently of positive buoyancy have undergone positive vertical displacement and vice versa. The latter makes sense when acceleration and displacement are of the same sign (no overshoot). Based on these assumptions, they deduced constraints on the distribution of samples in Paluch diagrams. In their paper, observations are limited to parcels with liquid water ("cloudy parcels") because of the difficulties in measuring humidity in unsaturated air. Nevertheless, the same argument could be extended to non-cloudy samples. No instance of buoyancy sorting is found in the RACORO observations. One such instance is found in our LES (Fig. 2a), where both cloudy and non-cloudy samples mostly fall in the allowed regions, as in shadings. Such instances are rare in our LES however. Likely reasons for the rarity include a) surrounding environment is horizontally heterogenous, b) the assumptions are not met due to the presence of overshooting updrafts/downdrafts, which have opposite signs of buoyancy and vertical displacement due to inertia and possible downward force of perturbation pressure gradient. The cloud-layer heterogeneity is discussed in section 5. Here we focus on the overshooting.

Level 1 on May 6 (Fig. 1b) and levels 1, 2 and 3 on June 9 (Fig. 1d) are likely instances of downdraft overshooting in that the sample lines extend beyond density isopleths (in other words, the upper portion of the samples lies above the density isopleth), which suggests that the drier source of the two-point mixing is more buoyant and therefore higher than the observation level. We infer that mixing above the observation level produces negatively buoyant mixture, which later descends and overshoots its LNB and gets observed with positive buoyancy. Similar features are found in the LES and shown in Fig. 2b. Parcels at 2460 m with $q_t$ smaller than 5 g/kg have positive buoyancy while apparently form a line pointing to an upper level (Fig. 2b), suggesting the case of downdraft overshooting. The altitudes of these parcels are tracked back by 1500 s in time using Lagrangian particles (Nie & Kuang, 2012) and shown in Fig. 2c. Parcels of $q_t < 5\ g/kg$ predominately originate from 200 ~ 1000 m above their height at $t = 0\ s$. Following Bretherton and Wyant (1997), buoyancy ($s_v'/c_p$) is decomposed as follows,

$$\frac{s_v{}'}{c_p} = \frac{s_{vl}}{c_p} - \frac{s_{vl}^{env}}{c_p} + 2.05\ \cdot q_l\ (g/kg)$$

where $s_{vl}$ is the virtual liquid static energy, which is conserved during adiabatic processes and mixing, $s_{vl}^{env}$ is the domain average of $s_{vl}$, $q_l$ is the liquid water content, and $c_p$ is the specific heat of dry air at constant pressure. The source of downdraft ($q_t < 5\ g/kg$) is divided into two categories based on their heights at $t = -1500\ s$ (Upper branch: $H > 2460\ m$; Lower branch: $H \leq 2460\ m$) to roughly distinguish between updrafts and entrained air. The buoyancy terms and vertical gradient of perturbation pressure ($-dp'/dz \cdot T_v/\rho g$ where $p'$ is the perturbation pressure, $T_v$ is virtual temperature, $\rho$ is density and $g$ is the gravitational acceleration constant) of each category are shown in Fig. 2d. The upper branch undergoes a decrease of $s_{vl}$ since $t = -400\ s$, downward force of the pressure gradient since $-200\ s$ and an overcompensating increase of $s_{vl}^{env}$. The lower branch experiences an accumulation and dissipation of liquid water content from $-600\ s$ to $-200\ s$, a rapid increase of $s_{vl}$ since $-400\ s$, a drop of $s_{vl}^{env}$ till $-200\ s$ and subsequent recovery which is concurrent with the upper branch, and the same downward pressure gradient force as that of the upper branch. A picture for intuition draws as follow: the lower branch (updrafts)

ascends when water vapor condenses, makes its way to the upper branch (entrained air) where it mixes; liquid water evaporates and reduces the buoyancy of the mixture, along with the downward force of perturbation pressure gradient sinks the mixture.

## 4 Updraft dilution

We have pointed out in section 3.1 that two-point mixing lines commonly show up in Paluch diagrams. The relative location of these two-point mixing lines and the surface measurements can inform us about updraft dilution, based on the following arguments. Suppose the surrounding environment is horizontally uniform and that there is no substantial downdraft, any sample at a sampling level has to lie within the region encompassed by the vertical sounding profile and a line segment connecting the surface condition and the current height on the vertical sounding profile. Therefore, if samples are right on the line segment, they must only be mixture of the sampling level and the surface but nothing else in between. In other words, no updraft reaches the sampling level after dilution. Fig. 1 includes the surface measurements at the CF concurrent with the aircraft samples. Out of the analyzed 11 instances of two-point mixing scenario, there are 5 instances (level 1 on May 6 (Fig. 1b), levels 4 and 5 on June 11 (Fig. 1e), levels 1 and 5 on May 24 (Fig. S2d)) where the two-point mixing lines point right toward the surface measurements. This is in contrast to the common belief of gradual dilution to updrafts (e.g., Bretherton et al., 2004).

Note that here the updraft dilution includes incorporation of environment air into an updraft from surface all the way up to the level of observation, different from Taylor and Baker (1991) where only mixing from the cloud base up is considered. Nevertheless, the good alignment between the sample lines and surface conditions in many instances of Fig. 1 suggests that neither dilution below the cloud base nor from the cloud base to the observation levels is significant.

There are also instances with the two-point mixing line pointing to the left (levels 2 and 3 of June 9 (Fig. 1d), level 4 of June 12 (Fig. 1f)) or to the right of surface measurements (levels 1 and 2 of June 12 (Fig. 1f), level 6 on May 23 (Fig. S2c)). While the former could be the case of nonzero updraft dilution, both could simply be a result of rapid drifting of surface conditions. Drifting of surface conditions is also apparent on level 2 on March 30 (Fig. 1a), only the earliest measurement of which (the leftmost yellow diamond in Fig. 1a) lies right on the two-point mixing line.

We clarify that the updraft dilution we detect here requires that the diluted updraft continues to rise, after mixing, for a noticeable distance, in the sense that the properties of the environment has noticeably changed. Our analyses of in situ measurements suggest that updrafts, once diluted, likely stop and detrain within a short distance. There are also instances in our LES with a homogenous surface showing no clear evidence of updraft dilution (Fig. S3).

Note that we are comparing aircraft samples against concurrent surface measurements. The conclusion still holds if we account for the updraft ascending time by assuming an updraft ascending velocity of 4 m/s and using earlier surface measurements accordingly.

## 5 Surface Heterogeneity

The LES case is validated against the entire flight path at 684 hPa on May 22 in Fig. 3, which is the highest horizontal path of the day, and shows representatively large horizontal variations of moisture. The sampling height (2620 m) in the LES is 400 m lower than the

flight level (~3000 m) to account for a lower cloud top in the LES. Both observations (Fig. 3a) and the LES with homogenous surface fluxes (Fig. 3b) show features of two-point mixing and neutral buoyancy. However, the variation of moisture along the density isopleth is significantly underrepresented in the LES. Fig. 3d shows a 50% fluctuation of surface latent heat flux from observations (Shi & Long, 2002) on the sampling path around 2 hours before sampling. Similar magnitude of fluctuation of surface heat fluxes is also present on the length scale of sampling track (but not exactly on the track) during the sampling. When this heterogeneity is included in the LES in Fig. 3c, the variation of moisture along the density isopleth agrees much better with the observations. The larger variation of moisture along the density isopleth in the Fig. 3c can be understood with the following thought experiment. We break the previous LES domain into two domains according to their surface heat fluxes and run them separately. Because of the different surface heat fluxes, the cloud layers will be different between the two domains. And as a result, the same horizontal slice in the cloud layer would see different average moisture and buoyancy. Now we put the two domains back by concatenating them side by side. There will be horizontal gradients of both buoyancy and moisture in the cloud layer. However, because horizontal buoyancy gradient can be effectively removed by gravity waves ($t_{gravity} \propto L$, where $t_{gravity}$ is the time it takes gravity waves to remove the horizontal buoyancy gradient and L is the horizontal length scale) while moisture gradient has to be removed by turbulent diffusion ($t_{turbulence} \propto L^2$ where $t_{turbulence}$ is the time it takes to remove horizontal moisture gradient purely by turbulent mixing), the buoyancy gradient will be removed ahead of the moisture gradient on such a length scale (10 km). As a result, Fig. 3c shows greater horizontal variations of moisture than of buoyancy.

Fig. 3e compares the domain-averaged cloud fraction between the two LES. Despite the same average surface latent and sensible heat fluxes, the case with heterogeneous surface fluxes shows overall larger cloud fraction, possibly due to a secondary circulation driven by the surface heterogeneity and further feedback processes (e.g., Avissar & Schmidt, 1998; Lee et al., 2019).

## 6 Conclusions and Discussions

The shallow cumulus cases observed during the RACORO campaign are studied in the transformed Paluch diagram and with non-cloudy samples included. Four scenarios, namely, two-point mixing, neutral buoyancy, buoyancy sorting and downdraft overshooting are studied with aircraft measurements over horizontal flight paths and with a LES. The two-point mixing scenario is quite common and can be unambiguously distinguished from the buoyancy sorting scenario of Taylor and Baker (1991) with the transformed Paluch diagram. The neutral buoyancy, where samples lie along a constant density isopleth, is also common. The buoyancy sorting scenario of Taylor and Baker (1991) is not found in the RACORO observations and is also rare in the LES case. The presence of updraft dilution is examined with two-point mixing lines and surface measurements. We find no noticeable updraft dilution in around half of the instances (5 out of 11) of two-point mixing. Lastly, surface heterogeneity is shown to be an important source of horizontal moisture variation.

Our analyses validate selected conceptual models of the cloud-environment interaction, namely, lateral entrainment/detrainment (e.g., Blyth et al., 1988; Heus et al., 2008), buoyancy sorting (Taylor & Baker, 1991) and long-distance (up to 1000 m) subsidence after mixing (e.g., cloud-top entrainment, Paluch, 1979).

We also devise a new approach to detect updraft dilution, by including non-cloudy parcels in a transformed Paluch diagram. This is especially useful in shallow cumulus cases because usually measurements of cloudy air are limited in size and show little variation in moisture and temperature, making it virtually impossible to identify a convincing two-point mixing line.

It would be interesting to detect updraft dilution with the same technique for deep convection, where gradual updraft dilution has been assumed (e.g., Böing et al., 2014). Stronger updrafts in deep convection might be able to continue rising after being diluted, so our result that no noticeable updraft dilution observed in RACORO might not hold for deep convection, which warrants future studies.

Finally, we note the necessity to include surface heterogeneity in LES. Such heterogeneity is reflected on the cloud layer variation of moisture and cloud fraction, and may further cascade on other cloud microphysics and macrophysics processes, such as cloud radiative forcing, convective aggregation.

**Acknowledgments, Samples, and Data**

Observational data sets were obtained from the U.S. Department of Energy ARM Climate Research Facility (https://www.arm.gov/) and the RACORO Campaign (https://campaign.arm.gov/racoro/). Data displayed in this paper are available from https://doi.org/10.5281/zenodo.4095607. The computations in this paper were run on the FASRC Cannon cluster supported by the FAS Division of Science Research Computing Group at Harvard University. This work was supported by the Office of Biological and Environmental Research of the U.S. DOE under grant DE-SC0018120 as part of the ASR Program. We thank David Turner for valuable discussions of the AERI soundings and his generous efforts to produce updated AERI soundings, Satoshi Endo for his helpful comments on LES configurations, Andrew Vogelmann for providing the flight videos, Thijs Heus, Christopher Bretherton, Yunyan Zhang, David Romps for insightful discussions about gravity waves, and three anonymous reviewers for their detailed and constructive critiques.

## References


Avissar, R., & Schmidt, T. (1998). An evaluation of the scale at which ground-surface heat flux patchiness affects the convective boundary layer using large-eddy simulations. *Journal of the Atmospheric Sciences, 55*(16), 2666-2689.

Blyth, A. M., Cooper, W. A., & Jensen, J. B. (1988). A Study of the Source of Entrained Air in Montana Cumuli. *Journal of the Atmospheric Sciences, 45*(24), 3944-3964.

Boatman, J. F., & Auer Jr, A. H. (1983). The role of cloud top entrainment in cumulus clouds. *Journal of the Atmospheric Sciences, 40*(6), 1517-1534.

Böing, S. J., Jonker, H. J., Nawara, W. A., & Siebesma, A. P. (2014). On the deceiving aspects of mixing diagrams of deep cumulus convection. *Journal of the Atmospheric Sciences, 71*(1), 56-68.

Bony, S., & Dufresne, J. L. (2005). Marine boundary layer clouds at the heart of tropical cloud feedback uncertainties in climate models. *Geophysical Research Letters, 32*(20).

Bretherton, C. S., McCaa, J. R., & Grenier, H. (2004). A new parameterization for shallow cumulus convection and its application to marine subtropical cloud-topped boundary layers. Part I: Description and 1D results. *Monthly Weather Review, 132*(4), 864-882.

Bretherton, C. S., & Wyant, M. C. (1997). Moisture Transport, Lower-Tropospheric Stability, and Decoupling of Cloud-Topped Boundary Layers. *Journal of the Atmospheric Sciences, 54*(1), 148-167.

Collins, W. D., Rasch, P. J., Boville, B. A., Hack, J. J., McCaa, J. R., Williamson, D. L., et al. (2004). Description of the NCAR community atmosphere model (CAM 3.0). *NCAR Tech. Note NCAR/TN-464+ STR, 226*.

Dai, A. (2006). Precipitation characteristics in eighteen coupled climate models. *Journal of Climate, 19*(18), 4605-4630.

Del Genio, A. D. (2012). Representing the sensitivity of convective cloud systems to tropospheric humidity in general circulation models. *Surveys in geophysics, 33*(3-4), 637-656.

Endo, S., Fridlind, A. M., Lin, W., Vogelmann, A. M., Toto, T., Ackerman, A. S., et al. (2015). RACORO continental boundary layer cloud investigations: 2. Large-eddy simulations of cumulus clouds and evaluation with in situ and ground-based observations. *Journal of Geophysical Research: Atmospheres, 120*(12), 5993-6014.

Grabowski, W. W., & Pawlowska, H. (1993). Entrainment and mixing in clouds: The Paluch mixing diagram revisited. *Journal of Applied Meteorology, 32*(11), 1767-1773.

Guichard, F., Petch, J., Redelsperger, J. L., Bechtold, P., Chaboureau, J. P., Cheinet, S., et al. (2004). Modelling the diurnal cycle of deep precipitating convection over land with cloud-resolving models and single-column models. *Quarterly Journal of the Royal Meteorological Society: A journal of the atmospheric sciences, applied meteorology and physical oceanography, 130*(604), 3139-3172.

Heus, T., Dijk, G. v., Jonker, H. J. J., & Akker, H. E. A. V. d. (2008). Mixing in Shallow Cumulus Clouds Studied by Lagrangian Particle Tracking. *Journal of the Atmospheric Sciences, 65*(8), 2581-2597.

Jensen, J., Austin, P., Baker, M., & Blyth, A. (1985). Turbulent mixing, spectral evolution and dynamics in a warm cumulus cloud. *Journal of the Atmospheric Sciences, 42*(2), 173-192.

Khairoutdinov, M. F., & Randall, D. A. (2003). Cloud resolving modeling of the ARM summer 1997 IOP: Model formulation, results, uncertainties, and sensitivities. *Journal of the Atmospheric Sciences, 60*(4), 607-625.

LaMontagne, R. G., & Telford, J. W. (1983). Cloud top mixing in small cumuli. *Journal of the Atmospheric Sciences, 40*(9), 2148-2156.

Lee, J. M., Zhang, Y., & Klein, S. A. (2019). The effect of land surface heterogeneity and background wind on shallow cumulus clouds and the transition to deeper convection. *Journal of the Atmospheric Sciences, 76*(2), 401-419.

Lin, J.-L. (2007). The double-ITCZ problem in IPCC AR4 coupled GCMs: Ocean–atmosphere feedback analysis. *Journal of Climate, 20*(18), 4497-4525.

Lin, J.-L., Kiladis, G. N., Mapes, B. E., Weickmann, K. M., Sperber, K. R., Lin, W., et al. (2006). Tropical intraseasonal variability in 14 IPCC AR4 climate models. Part I: Convective signals. *Journal of Climate, 19*(12), 2665-2690.

Malinowski, S. P., & Pawlowska, H. (1989). On estimating the entraininent level in cumulus clouds. *Journal of the Atmospheric Sciences, 46*(15), 2463-2465.

Mechoso, C. R., Robertson, A. W., Barth, N., Davey, M., Delecluse, P., Gent, P., et al. (1995). The seasonal cycle over the tropical Pacific in coupled ocean–atmosphere general circulation models. *Monthly Weather Review, 123*(9), 2825-2838.

Nie, J., & Kuang, Z. (2012). Responses of shallow cumulus convection to large-scale temperature and moisture perturbations: A comparison of large-eddy simulations and a convective parameterization based on stochastically entraining parcels. *Journal of the Atmospheric Sciences, 69*(6), 1936-1956.

Paluch, I. R. (1979). The Entrainment Mechanism in Colorado Cumuli. *Journal of the Atmospheric Sciences, 36*(12), 2467-2478.

Reuter, G., & Yau, M. (1987). Mixing mechanisms in cumulus congestus clouds. Part I: Observations. *Journal of the Atmospheric Sciences, 44*(5), 781-797.

Shi, Y., & Long, C. (2002). Best Estimate Radiation Flux Value-Added Procedure. Algorithm Operational Details and Explanations. *ARM Tech.Rep. TR-008, U.S. Dep. of Energy, Washington, D. C.*

Siebesma, A. P., Bretherton, C. S., Brown, A., Chlond, A., Cuxart, J., Duynkerke, P. G., et al. (2003). A large eddy simulation intercomparison study of shallow cumulus convection. *Journal of the Atmospheric Sciences, 60*(10), 1201-1219.

Taylor, G. R., & Baker, M. B. (1991). Entrainment and Detrainment in Cumulus Clouds. *Journal of the Atmospheric Sciences, 48*(1), 112-121.

Vogelmann, A. M., Fridlind, A. M., Toto, T., Endo, S., Lin, W., Wang, J., et al. (2015). RACORO continental boundary layer cloud investigations: 1. Case study development and ensemble large-scale forcings. *Journal of Geophysical Research: Atmospheres, 120*(12), 5962-5992.

Vogelmann, A. M., McFarquhar, G. M., Ogren, J. A., Turner, D. D., Comstock, J. M., Feingold, G., et al. (2012). RACORO extended-term aircraft observations of boundary layer clouds. *Bulletin of the American Meteorological Society, 93*(6), 861-878.

Zhang, Y., & Klein, S. A. (2013). Factors controlling the vertical extent of fair-weather shallow cumulus clouds over land: Investigation of diurnal-cycle observations collected at the ARM Southern Great Plains site. *Journal of the Atmospheric Sciences, 70*(4), 1297-1315.

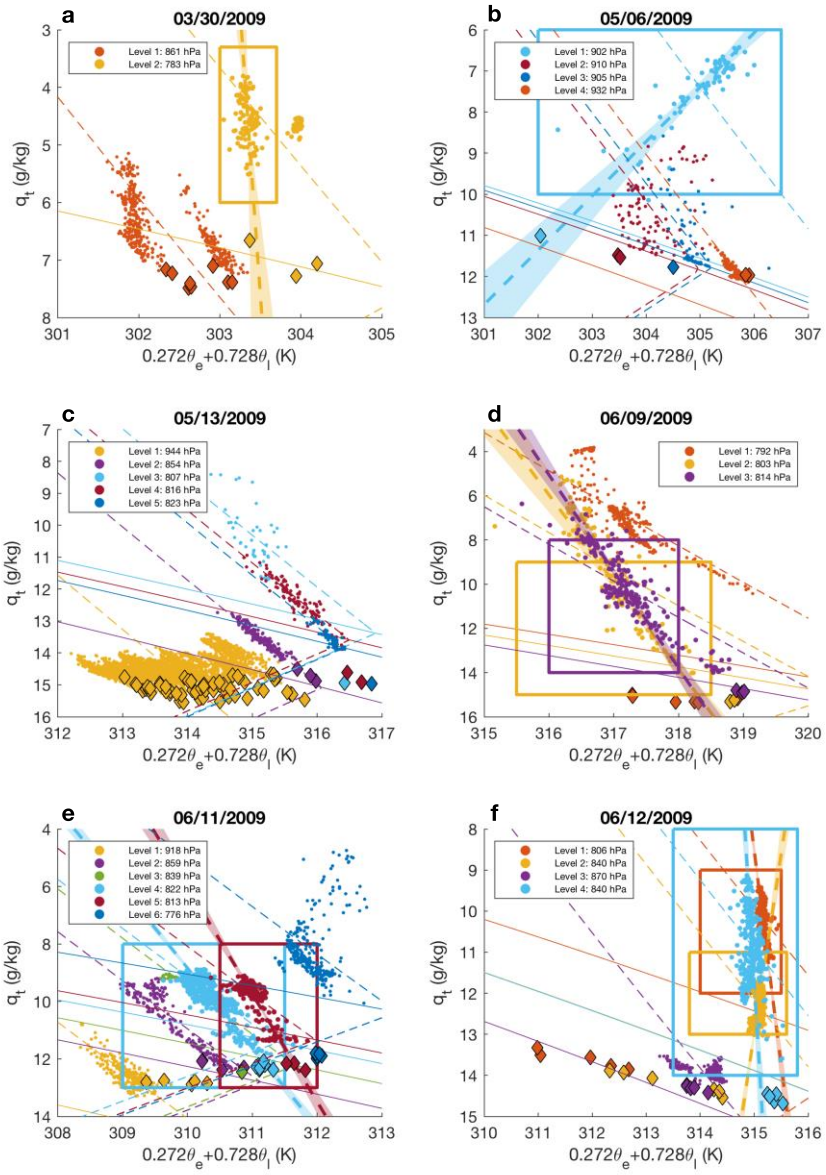


**Fig. 1**. Samples from 6 flights of the RACORO campaign in transformed Paluch diagrams. Titles state the dates of flight. Samples (dots), density isopleths (thin dashed lines), saturation lines (solid lines) and concurrent 1-min averaged surface measurements at the CF (diamonds) are color coded by the corresponding altitudes. The density isopleths are calculated based on the average density of samples from each path. The legends state the average pressure of each path. Two-point mixing lines (thick dashed lines) are the linear regression of $0.272 \cdot \theta_e + 0.728 \cdot \theta_l$ against $q_t$ of samples encompassed by the rectangles of the corresponding colors. Shading shows the 5 ~ 95% confidence interval of a linear regression line.

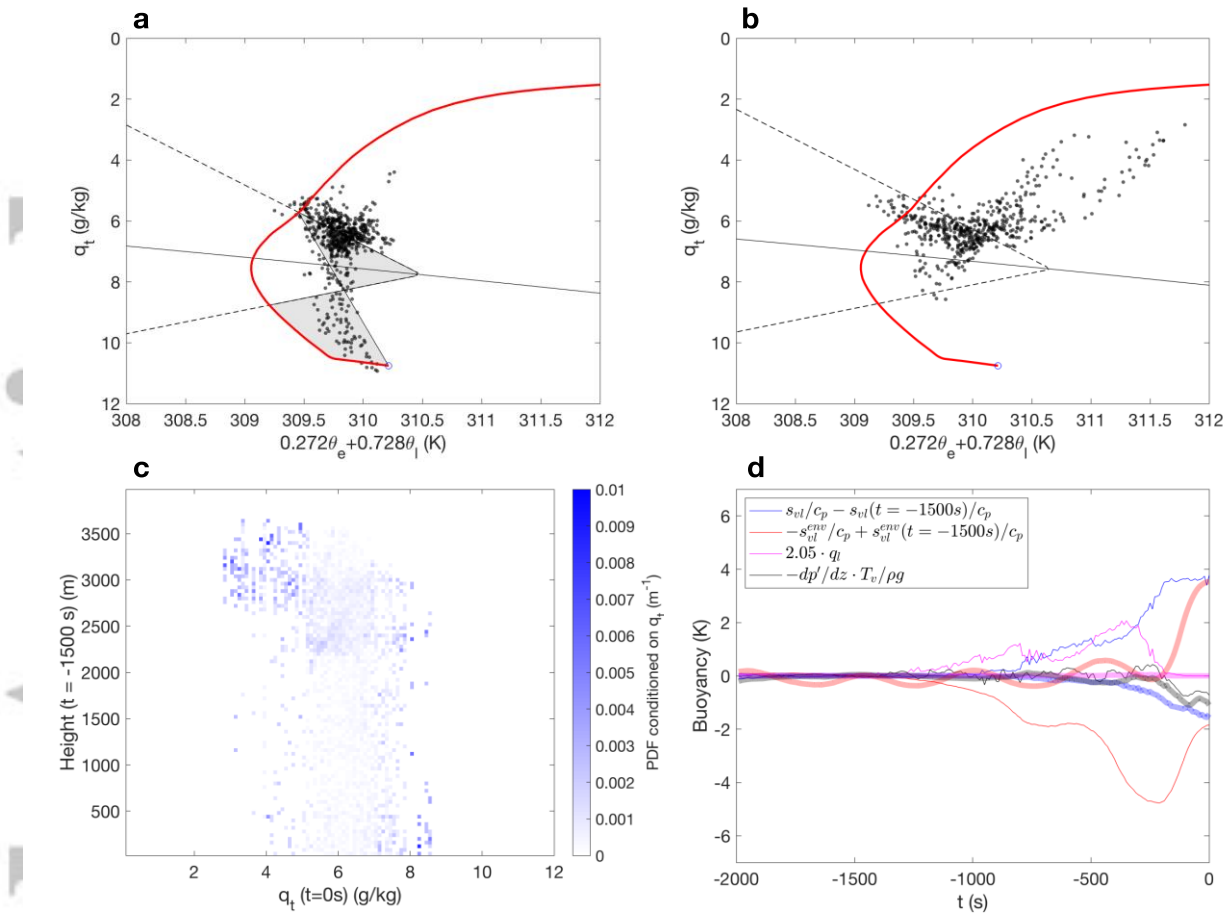


**Fig. 2**. a) An instance of buoyancy sorting from the LES as in Taylor and Baker (1991). The shaded region indicates a dynamical constraint on samples' distribution: parcels are theoretically restricted to be within the shaded region in the buoyancy sorting scenario of Taylor and Baker. b) an instance of downdraft overshooting from the LES at 2460 m in altitude with homogenous surface. Samples (black dots), density isopleths (dashed lines), saturation lines (black lines), surface conditions (blue circles) and vertical profiles (red lines) are plotted in a) and b). c) Probability density function (conditioned on $q_t$) of parcels at 2460 m (t = 0 s) as a function of $q_t$ (t = 0 s) and H (t = -1500 s). d) Buoyancy terms and vertical gradient of perturbation pressure ($-dp'/dz \cdot T_v/\rho g$) as a function of time are shown for an upper branch ($H\ (t = -1500\ s) > 2460\ m$, thick lines) and a lower branch ($H\ (t = -1500\ s) \leq 2460\ m$, thin lines) of downdraft ($q_t < 5\ g/kg$).

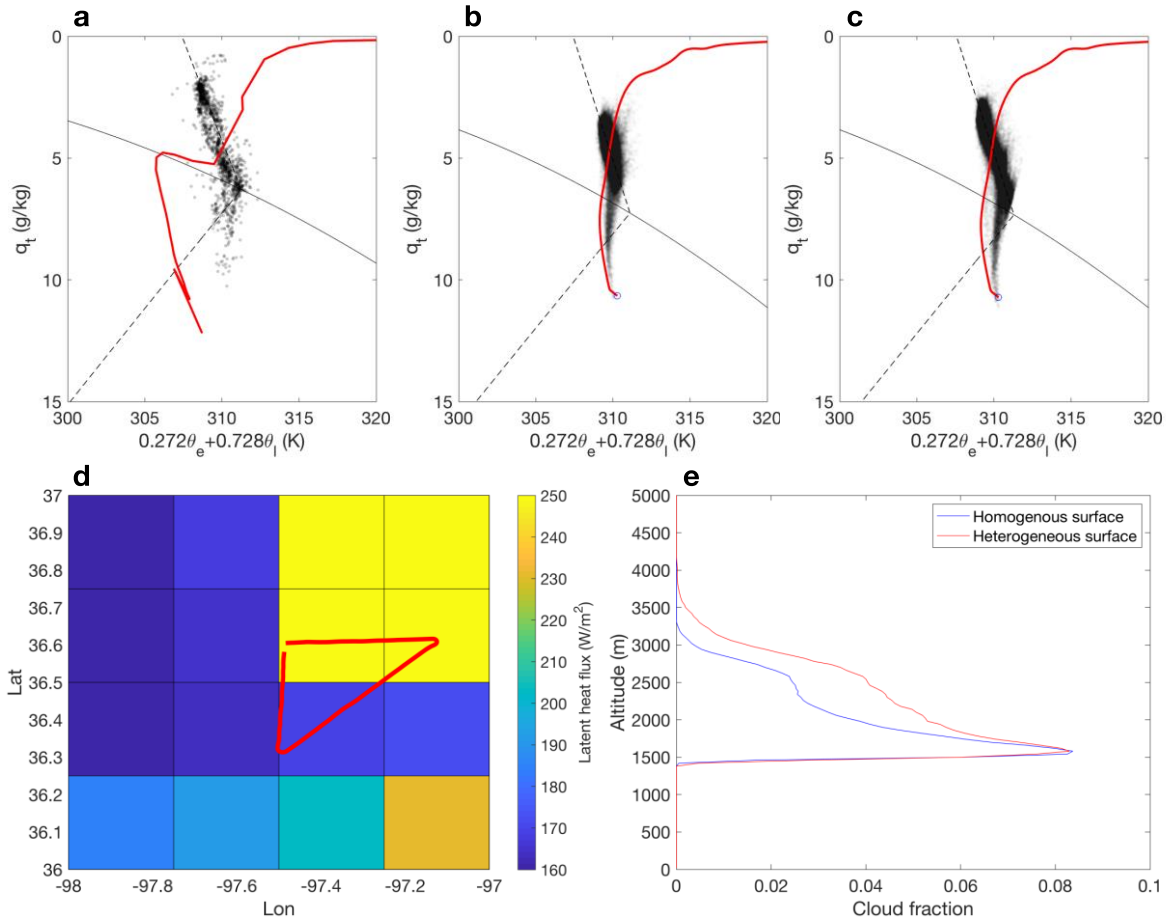


**Fig. 3**. Transformed Paluch diagrams of a) measurements over the entire horizontal path at 684 hPa on May 22 of RACORO, b) domain samples at 2620 m in the LES with a homogenous surface and c) domain samples at 2620 m in the LES with a heterogeneous surface. The vertical profile in a) is retrieved by AERI. d) Best estimate of the surface latent heat flux (Shi & Long, 2002) at 9 am LT. The red line indicates the aircraft track. e) Cloud fraction of the LES at 11:30 am with homogenous and heterogeneous surfaces as a function of altitude.